L. Zhang, M. Nikolopoulou, S. Guo & D. Song. Impact of LCZs spatial pattern on urban heat island: a case study in Wuhan, China, *Building and Environment*, 2022. https://doi.org/10.1016/j.buildenv.2022.109785

Impact of LCZs spatial pattern on urban heat island: a case study in Wuhan, China

Li Zhang[a, b, c, *], Marialena Nikolopoulou[b], Shujing Guo[a], Dongyi Song[a]

a. Collage of Horticulture and Forestry Sciences, Huazhong Agricultural University, 1Shizishan Street, Wuhan 430070, China

b. Kent School of Architecture & Planning, University of Kent, Canterbury, Kent CT2 7NR, UK

c. Key Laboratory of Urban Agriculture in Central China, Ministry of Agriculture and Rural Affairs, P.R.China

* Zhangli09@mail.hzau.edu.cn

Abstract: Based on World Urban Database and Access Portal Tools (WUDAPT), this study mapped Local Climate Zones (LCZs) in Wuhan in 2020 and detected surface urban heat island intensity (SUHII) within LCZs in day/night of all seasons through Moderate Resolution Imaging Spectroradiometer (MODIS) land products. Four landscape metrics were used to explore spatial heterogeneous effects of LCZs on SUHII by Geographically weighted regression (GWR) model. Results showed that LCZs map can be used to describe the thermal environment in Wuhan. SUHII difference among LCZs was stronger in spring and summer, while less in winter. SUHII difference of the same LCZ was found in three districts in Wuhan. SUHII of most other built classes in Hankou were higher than Wuchang and Hanyang. SUHII within LCZ G in Wuchang was the lowest in daytime of all seasons but the highest at night of all seasons. LCZ 2, LCZ 4, LCZ 5, LCZ 8 and LCZ H had strong positive correlation with SUHII and LCZ D and LCZ G had significant negative correlation with SUHII. Percentage of landscape (PLAND) of LCZs had stronger impact on SUHII than Contagion index (CONTAG), Shannon's diversity index (SHDI) and Area-weighted mean shape index (SHAPE_AM) of LCZs. PLAND of LCZ 8 had strong impact on increasing SUHII in daytime of all seasons, while PLAND of LCZ 2, LCZ 4 and LCZ 5 showed obvious influence on increasing SUHII at night of all seasons. LCZ D had strong impacts on decreasing SUHII in daytime of all seasons and less cooling impacts at night of all seasons. LCZ G showed strong cooling impacts on SUHII in day/night time of all seasons except winter nighttime. SHDI richness of LCZs in analysis unit helped alleviate SUHII. High CONTAG of LCZ with high LST increase SUHII, while High CONTAG of LCZ with low LST decrease SUHII. Very regular shape of LCZ built classes increased the SUHII, while less fragmented of LCZ land cover classes decreased the SUHII.

Key words: LCZs, urban heat island, spatial pattern, day/night of all seasons

1.Introduction

With the rapid urbanization, climate change is an undeniable challenge humanity is facing. According to IPCC 2022, one of the impacts of climate change is the increasing frequency and intensity of hot extremes on land. In the summer season in 2022, the extreme heat in south China lasts at least for 70 days (Andrew, 2022), and an increasing number of cities are affected by very high temperatures close to 40°C in summer in 2022 (Yusha et al., 2022). Shangguan News reported that, as of August 10, 2022, Shanghai had seen 37 hot temperature days this summer, including more than 37℃ of scorching heat in 21 days, and the extreme heat of more than 40℃ has reached five days (Ting, 2022). High temperature caused drought in many places and over energy consumption, which had the negative influences on urban living (Nectar, 2022).

Extensive research on urban high temperature in recent years has found that urbanization influences the land cover apparent change which causes the high temperature in urban environments (Aslam & Rana, 2022). Stewart and Oke (Stewart & Oke, 2012) proposed the concept of the Local Climate Zone (LCZ) as a climate-based classification of urban and rural areas for thermal study. Based on the similar characteristic of land cover, material, structure and human activity, the areas are classified into 17 LCZs including 10 built classes and 7 land cover classes (Geletič, Lehnert, Savić, & Milošević, 2019; Zhao, Jensen, Weng, Currit, & Weaver, 2019; Y. Zhou et al., 2021). It provides a framework to describe the land surface condition in urban and rural area from the thermal climate aspect (Stewart & Oke, 2012).

Previous studies of LCZs were mainly mapped based on the World Urban Database and Access Portal Tools (WUDAPT) and GIS-based method (Aslam & Rana, 2022; Quan & Bansal, 2021). WUPAPT was developed by Bechtel to map LCZs through Landsat images, training area samples and System for Automated Geoscientific Analyses (SAGA) tool (Anjos, Targino, Krecl, Oukawa, & Braga, 2020; X. Zhou, Okaze, Ren, Cai, Ishida, & Mochida, 2020). The GIS-based method relied on the data of urban developed indexes correlating with thermal environment, such as aspect ratio, impervious surface fraction, building heigh, surface albedo, (Quan & Bansal, 2021; J. Wu, Liu, & Wang, 2022; J. Yang et al., 2021; Y. Zhou et al., 2021), which are not available to the public in most Chinese cities. Based on two mapping LCZs methods, much precise data with high-resolution images, lidar points and other classifiers and algorithms method, such as residual convolutional neural network, Naïve bayes, support vector machine, were explored to improve the accuracy of LCZs mapping (Hay Chung, Xie, & Ren, 2021; Hidalgo et al., 2019; Kim, Jeong, & Kim, 2021; Liu & Shi, 2020; Ma, Yang, Zhou, Lu, & Yin, 2021; Xu et al., 2021; Yoo, Han, Im, & Bechtel, 2019; Zhao et al., 2019; L. Zhou et al., 2022).

Studies mapped LCZs in cities of different macroclimate regions (arid, subtropical, tropical, temperate, cold, etc.) (Eldesoky, Gil, & Pont, 2021; Kotharkar, Ghosh, & Kotharkar, 2021; C. Wang et al., 2018; J. Wu et al., 2022), or even under cloudy or windy conditions to verify that the LCZ framework was suitable (Beck et al., 2018; X. Zhou, Okaze, Ren, Cai, Ishida, Watanabe, et al., 2020). Land surface temperature (LST) or surface urban heat island (SUHI) difference within LCZs was detected in summer, or day/night, or seasonal time in one year or multi-year (Du, Chen, Bai, & Han, 2020; Ma et al., 2021; J. Yang et al., 2021; X. Yang, Peng, Chen, Yao, & Wang, 2020; L. Zhou et al., 2022). Results proved that LST of LCZs showed the diurnal and seasonal differences. It was observed that the highest difference of SUHI within LCZs occurred in summer daytime and lowest in winter daytime (Geletič et al., 2019), and higher LST or SUHI were found in LCZ built classes. However, the LZC type from LCZ 1 to LCZ 10 having the highest LST or SUHI in different cities was not same for the various regional climate environments, and also changed from seasons and day/night (Wang et al., 2018). Studies have used the LCZ framework for both intra-city heat island as well as for multi-city studies at a continental scale (Chen, Yang, Ren, Jeong, & Shi, 2021), and found that latitude, altitude, and the distance to coastline had a strong relation with air temperature within LCZs.

The relationship between urban morphology and thermal environment was also detected through LCZ mapping (J. Yang et al., 2019; Wang et al., 2022). Present studies showed that the detailed urban morphology of LCZ built type in different city was not as same as the original criterion proposed by Steward and Oke because the various urban development (X.

Zhou, Okaze, Ren, Cai, Ishida, Watanabe, et al., 2020). Researchers also noticed that spatial pattern of LCZs had relation with LST. Landscape metrics such as percentage of landscape (PLAND), aggregation Index (AI), number of patches (NP), mean patch area (AREA_MN), total core area (TCA), shannon's diversity index (SHDI) were used to describe the spatial pattern of LCZs. It was found that PLAND, AI, NP of built-up type, vegetation and water had correlation with LST in September in Bandung, Indonesia (Simanjuntak, Kuffer, & Reckien, 2019).

Among previous studies, some heat environment studies based on LCZs were done in Wuhan (Shi et al., 2021; Y. Wang, Zhan, & Ouyang, 2017; Wang et al., 2022). Researchers detected seven LCZ types with great heating or cooling influence on urban temperature and explored the impact of metrics of seven LCZ types on temperature (Y. Wang, Zhan, & Ouyang, 2017). However, LCZs in this research was mapped in 2013 which wasn't suit for present because the fast development in Wuhan during the past years. The research focused on correlation between landscape metrics of each LCZ type and LST, and ignored the influence of spatial pattern between LCZs. Wang (2022) used the geographic detector model to explore the driving factors of LST spatial difference from nature and social aspects. The results showed that LCZ had the most explanatory power for the LST spatial variation. While, most studies focused on the LST within LCZs in seasonal daytime and neglected LST changes of LCZs at nighttime in Wuhan (Shi et al., 2021; Y. Wang, Zhan, & Ouyang, 2017; Wang et al., 2022). Furthermore, they seldomly explored the extent to which the LCZ impact on the SUHII and detect these diurnally at different seasons.

The aim of the current study is to clarify the LCZ spatial character and its influence on thermal environment using Wuhan as a case study. More specifically it focuses on: 1) mapping LCZs in Wuhan in 2020; 2) detecting the SUHII within LCZs in day/night of all the seasons to explain the thermal environment of LCZs; and 3) exploring the LCZ spatial pattern and its impacts on SUHII diurnally at different seasons to clarify the main influences from spatial pattern aspect. Results would help planners and other officials to understand the main LCZ type for thermal environment in Wuhan, which could then be used to guide development in the future to get a better urban climate in Wuhan.

2.Method

2.1 Study area

Wuhan is located in central China (30°35′N, 114°17′ E), and is also called as "hundreds of lakes" due to the many natural lakes and rivers in the city area. Wuhan has subtropical monsoon humid climate (Koppen classification Cf), characterized by abundant rainfall, sufficient sunshine, hot summer and cold winter. Winter covers from December to February with an average temperature of 3°C and summer covers from June to September with an average temperature of 29.8°C (Zhang, Zhan, & Lan, 2018). Wuhan metropolitan area is selected as the study area because it is a main urban functional area and also the urban development area. Eight million residents live in the metropolitan area of 3,261 km^2. Yangzi River crossing the city from south to north and Han River divide the city into three districts (Hankou, Wuchang and Hanyang). Wuhan is mainly concentrated in Hankou, which is a major economic and commercial area, and also the location of the old city. Hanyang and Wuchang have more lakes than Hankou. The biggest industry factory, Wuhan Iron and Steel Factory, is located in north of Wuchang.

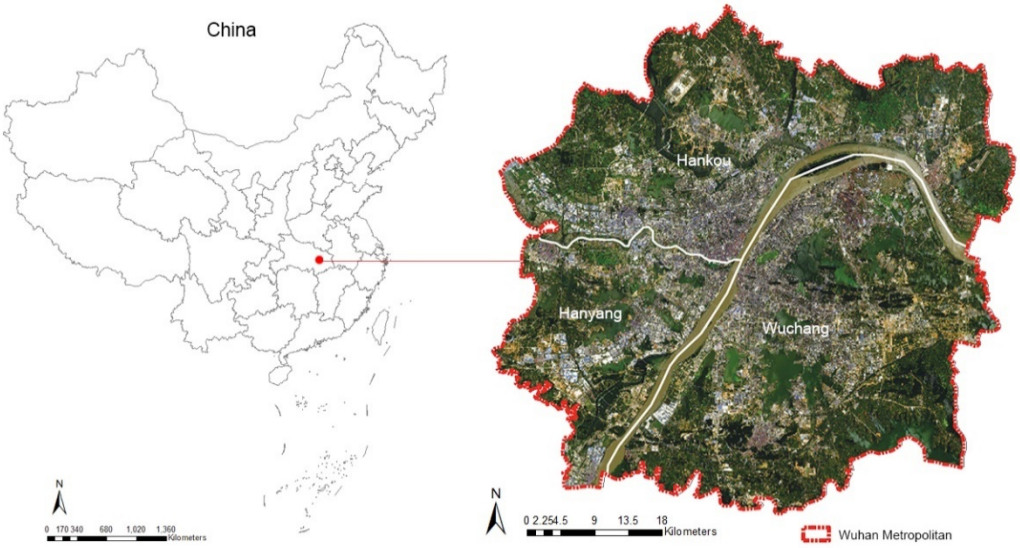

Fig. 1. Study area and three districts in Wuhan

2.2 Data sources and processing

In this study, data processing included three steps (Fig. 2). The first step was mapping LCZs. The second step was day/night seasonal SUHII analysis based on LCZs in three districts in Wuhan. The last step was LCZs spatial pattern variable selection and influence analysis on surface urban heat island intensity (SUHII).

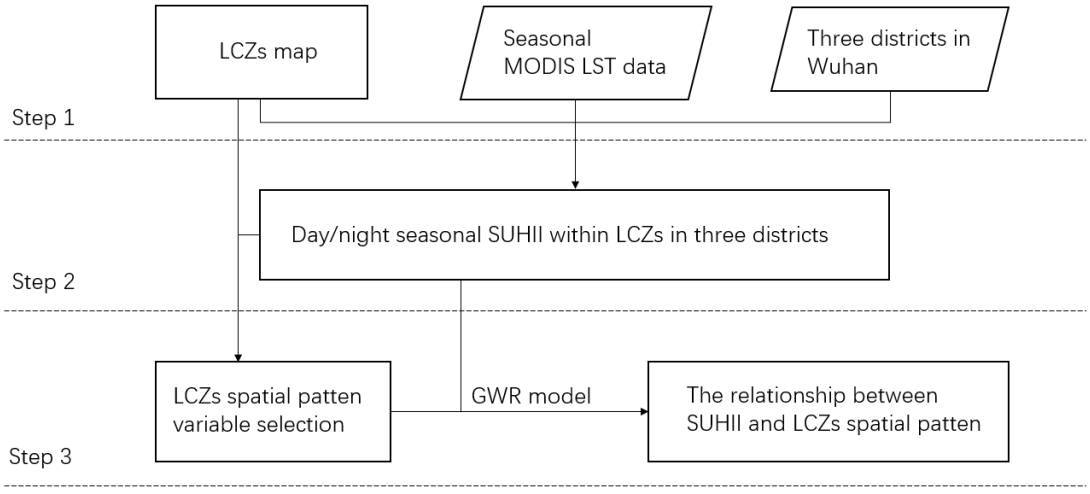

Fig. 2. The methodological flowchart of this study.

2.2.1 LCZ classification

World Urban Database and Access Portal Tool (WUDAPT) is used to map the LCZs based on a machine learning algorithm such as random forest classifier for satellite images (Anjos et al., 2020; Aslam & Rana, 2022; Emery et al., 2021). First, cloud less Landsat 8 image in 2020 was synthesized from Google Earth Engine (GEE) platform and selected as input data for mapping LCZs of the year 2020.

Second, 620 training samples were collected across the metropolitan area in Google Earth according to the characteristic of each LZC type. Except LCZ 7 (Lightweight low-rise),

all other LCZ types had been detected in metropolitan area. Wuhan is in rapid development. There are large land surface areas, such as in Fig. 3. which are in construction process, and these land surfaces are often in a process of dynamic change. In the early stage (Fig. 3(a)), it is mainly soil, and it is similar to bare soil or sand. In the middle stage (Fig. 3(b)), it is a mixture of soil and building materials. In the later stage (Fig. 3(c)), it is similar to the middle stage and the difference is that the basic outline of the building can already be seen. Therefore, on the basis of the original LCZ classification, this study defines such land surface as the construction area (LCZ G). Random 70% samples were used for classification and 30% samples were used to evaluate the classification accuracy.

Fig. 3. Samples of construction area from Google Earth.

Resampled Landsat 8 image of 2020 (at 100 m resolution) and 424 training samples were used in SAGAGIS software (X. Zhou, Okaze, Ren, Cai, Ishida, Watanabe, et al., 2020). A 3 * 3 pixels majority filter (500*500 m) was used to erase fragments during post-processing (J. Wang, Qingming, Guo, & Jin, 2016). The LCZ map in 2020 of Wuhan metropolitan area was generated.

2.2.2 Day/night seasonal LST/SUHI processing

The MODIS LST product (MOD11A1) was selected in this study because it contains day and night LST data. To map LST in metropolitan area in four seasons, we deleted the data with rain and selected continuous less cloudy images in 2020. Cloud-free composite images of each season in 2020 were acquired in GEE platform through ee.Reducer and ee.Imagecollection tool (Li, Stringer, & Dallimer, 2022). Composite images from February 18 to 19, April 23 to 28, August 26 to 28, December 03 to 13 represented winter, spring, summer and autumn respectively. Each season day and night MODIS data were calculated for LST using equation (1).

LST = 0.02*DN-273.15 equation (1)

where DN is the pixel value of MOD11A1.

Using statistical analysis, we compared LST within LCZs to evaluate the thermal difference between LCZs in Wuhan. ANOVA test was used to detect the significance of LST variance between LCZ groups (Emery et al., 2021; Kotharkar et al., 2021) and then Tamhane T2 test was selected to show which group have the difference.

To illustrate the day/night seasonal SUHII within LCZs, the SUHII was defined as the LST difference of a LCZ type when compared with LCZ D (low plants) (Jin et al., 2020; Li et al., 2022; X. Yang et al., 2018). The formula for acquiring SUHII was as follows:

$$SUHII_{LCZx} = LST_{LCZx} - LST_{LCZD} \quad \text{equation (2)}$$

where LCZ_x is a LCZ type in Wuhan, $SUHII_{LCZx}$ is SUHII in LCZ_x, LST_{LCZx} is LST value in LCZ_x, LST_{LCZD} is LST value in LCZ D.

2.2.3 LCZs spatial pattern variable selection

LCZs spatial pattern includes composition and configuration between LCZs (Wu et al., 2022). First, seven candidate landscape metrics that were significantly correlated with LST in previous studies were selected, namely percentage of landscape (PLAND), contagion (CONTAG), area-weighted mean patch shape index (SHAPE_AM), shannon's diversity index (SHDI), patch density (PD), aggregation Index (AI), total edge contrast index (TECI). Second, these metrics with annual mean variance inflation factor (VIF) higher than 10 were excluded to avoid multicollinearity. Finally, four landscape metrics including PLAND, CONTAG, SHAPE_AM, SHDI were finally selected to describe the LCZs spatial pattern. PLAND is an index showing the LCZs composition which was calculated in a class level, and the other three indexes showing the LCZs configuration which were calculated in a landscape level. Details can be seen in Table 1.

Table 1 Specific information on landscape metrics.

Metric	Formula	Description
percentage of landscape (PLAND)	PLAND = $P_i = \frac{\sum_{j=1}^{n} a_{ij}}{A}(100)$	The percentage of the landscape comprised of the corresponding patch type.
contagion (CONTAG)	CONTAG = $\left[1 + \frac{\sum_{i=1}^{m}\sum_{k=1}^{m}\left[(P_i)\left(\frac{g_{ik}}{\sum_{i=1}^{m} g_{ik}}\right)\right]\left[\ln(P_i)\left(\frac{g_{ik}}{\sum_{i=1}^{m} g_{ik}}\right)\right]}{2\ln(m)}\right](100)$	The extent to which patch types are aggregated or clumped.
area-weighted mean shape index (SHAPE_AM)	SHAPE_AM = $\sum_{i=1}^{k}\sum_{j=1}^{ni}\left(\frac{0.25P_{ij}}{\sqrt{a_{ij}}}\right)\left(\frac{a_{ij}}{A}\right)$	The average shape index of patches of the corresponding patch type, weighted by patch area so that larger patches weigh more than smaller patches.
shannon's diversity index (SHDI)	SHDI = $-\sum_{i=1}^{m}(P_i \ln P_i)$	The degree of diversity of patch types within units.

Note: P_i is the proportion of the landscape occupied by patch type i; a_{ij} is the area (m^2) of patch ij; A is the total landscape area (m^2); g_{ik} is the number of adjacencies (joints) between pixels of patch types i and k; m is the number of patch types present in the landscape; P_{ij} is the perimeter (m) of patch ij.

Moving window method was used to get the value of four indexes in Fragstats software. Based on the LCZs mapping at 100 *100 m resolution, four indexes were employed by using 10 parameters from 500 m to 5000 m (500 m as tolerance) as window radii. Built grids as same as the 10 parameters in ArcGIS to overlay it with the correspondent four indexes and SUHII, then to assign the grid units with their respective LCZs spatial pattern and SUHII. Spearman correlation analysis was employed between four indexes and SUHII at various window radii. The absolute correlation coefficients were compared to define the optimization window radii. As Fig. 4 shows, the strongest correlation between SHDI, CONTAG and SUHII were at 3000 m, and the strongest correlation between PLAND with SUHII was at 2000 m while the strongest correlation between SHAPE_AM with SUHII was at 1500 m. Considering four indexes, 1500 m was finally set as the window radii and grid scale for the following study.

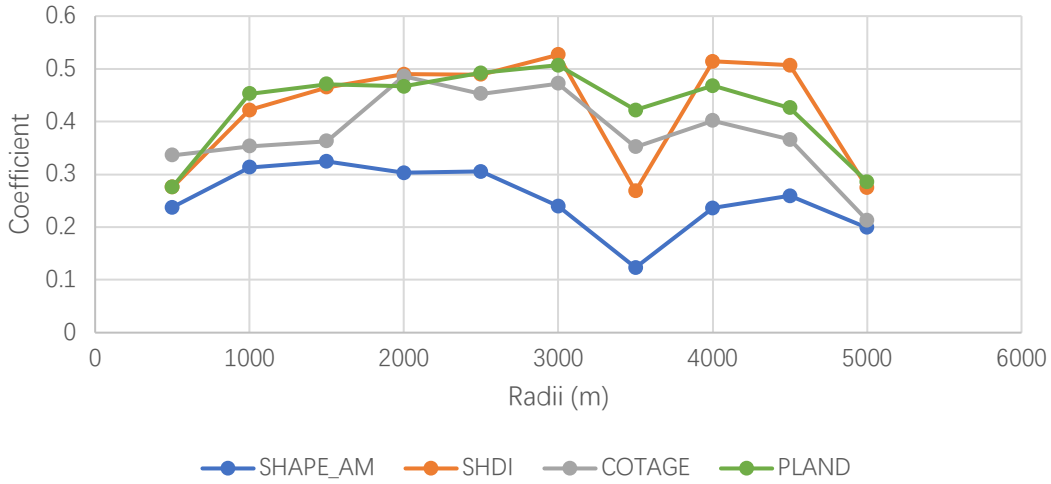

Fig. 4. The mean absolute value of the correlation between landscape indicators and SUHII.

PLAND in this study illustrates the LCZs composition. Studies have showed that LCZs has various impacts on SUHII. In this study, LCZ types which have strong effects on SUHII and with enough area proportion (above 0.1%) were chosen for the next step. Spearman correlation test was used between LST and PLAND of each LCZ type, and the coefficient larger than 0.4 was defined as the strong correlation between PLAND and LST (Table 2). Then, PLAND of LCZ 2, LCZ 4, LCZ 5, LCZ 8, LCZ D, LCZ G, LCZ H were selected for the following research.

Table 2 Correlation coefficient of PLAND within each LCZ type and SUHII

LCZs	Coefficient	LCZs	Coefficient	LCZs	Coefficient	LCZs	Coefficient
LCZ 1	0.099**	LCZ 2	0.423**	LCZ 3	0.296**	LCZ 4	0.552**
LCZ 5	0.557**	LCZ 6	0.142*	LCZ 8	0.584**	LCZ 9	0.038*
LCZ 10	0.223**	LCZ A	-0.267**	LCZ B	-0.153**	LCZ C	-0.281**
LCZ D	-0.494**	LCZ E	0.187**	LCZ F	0.104**	LCZ G	-0.435**
LCZ H	0.508**						

Note: ** represents $p < 0.01$ in the significance test.

2.2.4 Correlation analysis

Geographically weighted regression model (GWR) is a regression approach for the

geospatial nonstationary variables which was proposed by Brunsdon in 1996 (Lu, Charlton, Harris, & Fotheringham, 2014). Based on nonparametric local weighted regression, local regression coefficients are estimated for each spatial position in the study area which reflect the spatial differentiation characteristics of the explanatory variable on the dependent variable in the study area (Gao, Zhao, & Han, 2022). The formal of GWR is expressed as:

$$y_i = \beta_0(u_i, v_i) + \sum_{j=1}^{k} \beta_j(u_i, v_i) X_{ij} + \varepsilon_i \quad \text{equation (3)}$$

where y_i is the SUHII at location i, (u_i, v_i) is the coordinates of location i, X_{ij} is the spatial indexes at location i, β_0 and β_j are the estimated coefficients at location i, ε_i is the random error at location i.

Before employing GWR test, spatial autocorrelation analysis is required to illustrate how the variable is autocorrelated through space (Gao et al., 2022). In this study Global Moran's I was used in ArcGIS to investigate the spatial autocorrelation of variables. The formula of Moran's I is as follows:

$$I = \frac{n \sum_{i=1}^{n} \sum_{i=1}^{n} w_{ij}(x_i - \bar{x})(x_j - \bar{x})}{(\sum_{i=1}^{n} \sum_{i=1}^{n} w_{ij}) \sum_{i=1}^{n} (x_i - \bar{x})^2} \quad \text{equation (4)}$$

where n is the total number of the geographic units, x_i and x_j are the values at location i and j, w_{ij} is the spatial weight matrix between variable at location i and j. The value of Moran's I is from -1 to 1, closing 0 demonstrates no spatial autocorrelation. Besides, z-score and p-value are supplementary indicators to interpret the null hypothesis of no spatial autocorrelation. The original null hypothesis can be rejected as $|Z|$>1.96, and the Moran's I is statistically significant when p<0.05.

Prior to employ the correlations, the multicollinearity between all spatial indexes was tested. All spatial indexes were employed in multiple linear regression model and the variance inflation factor (VIF) less than 10 were applied to ensure no collinearity between indexes (Dewan et al., 2021; Gu & You, 2022).

3.Results

3.1 Mapping of LCZs

As shown in Fig. 5 and Table 3, LCZ mapping in Wuhan included 9 built classes, 7 land cover classes and a supplement class. LCZ 1 to LCZ 6 were concentrated in the central area along with Yangzi River and Han River. LCZ 1 covering 0.01% was the smallest one of built classes and was in Hankou district. LCZ 2 and LCZ 3 were most clustered in the old town, and covered 0.79 % and 1.24 % respectively. LCZ 4 and LCZ 5 locating in central city were the two large built classes, and covered 11.9 % and 4.91 % respectively. It illustrates that LCZ 4, the largest one of built classes, had been the dominated space in Wuhan. LCZ 6 covering 0.45 % located around lakes and most of them were on the periphery of the central area. LCZ 8 covering 5.29 % was another large built class and distributed along with the main road on the periphery of the central. LCZ 9 covered 0.02 % and LCZ 10 was mainly in Wuchang with 0.65 %.

Among land cover classes, LCZ D was the largest one (30.46 %) and distributed in patches at the periphery. LCZ G was the next large one (13.09 %), and compared with Wuchang and Hanyang district, less LCZ G was in Hankou district. LCZ A, LCZ B and LCZ C scattered in Wuhan with area proportion 6.25 %, 9.68 % and 3.7 % respectively. LCZ E was the smallest one among land cover classes with area proportion 0.28 %. It is noticed that LCZ F and LCZ H were the developing space in Wuhan distributing in the outside of the central area, and covered

6.9 % and 4.4 % respectively.

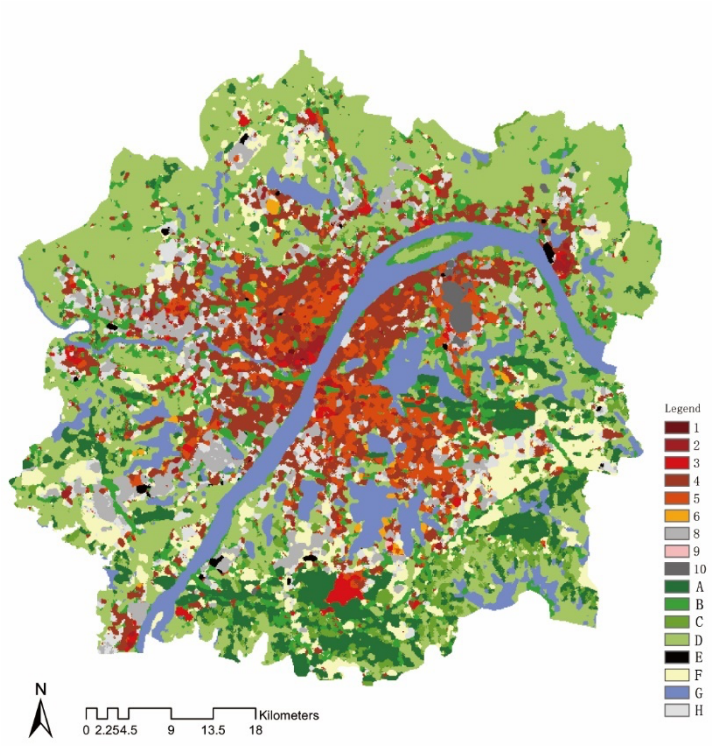

Fig. 5. LCZ map of Wuhan in 2020

Table 3 Land area proportion of each LCZ type.

LCZ	Area Proportion (%)	LCZ	Area Proportion (%)
LCZ 1 (compact high-rise)	0.01	LCZ A (dense trees)	6.25
LCZ 2 (compact mid-rise)	0.79	LCZ B (scattered trees)	9.68
LCZ 3 (compact low-rise)	1.24	LCZ C (bush, scrub)	3.70
LCZ 4 (open high-rise)	11.9	LCZ D (low plants)	30.46
LCZ 5 (open mid-rise)	4.91	LCZ E (bare rock or paved)	0.28
LCZ 6 (open low-rise)	0.45	LCZ F (bare soil or sand)	6.9
LCZ 8 (large low-rise)	5.29	LCZ G (water)	13.09
LCZ 9 (sparsely built)	0.02	LCZ H (construction)	4.40
LCZ 10 (heavy industry)	0.65		

The accuracy of each LCZ is presented in Fig. 6. The overall accuracy and Kappa coefficient were 83.8 % and 0.824, which are above the accuracy standardize of LCZ map (50% and 0.5, respectively) proposed by Bechtel (Bechtel et al., 2019). These indicated that the result of LCZ mapping was satisfactory.

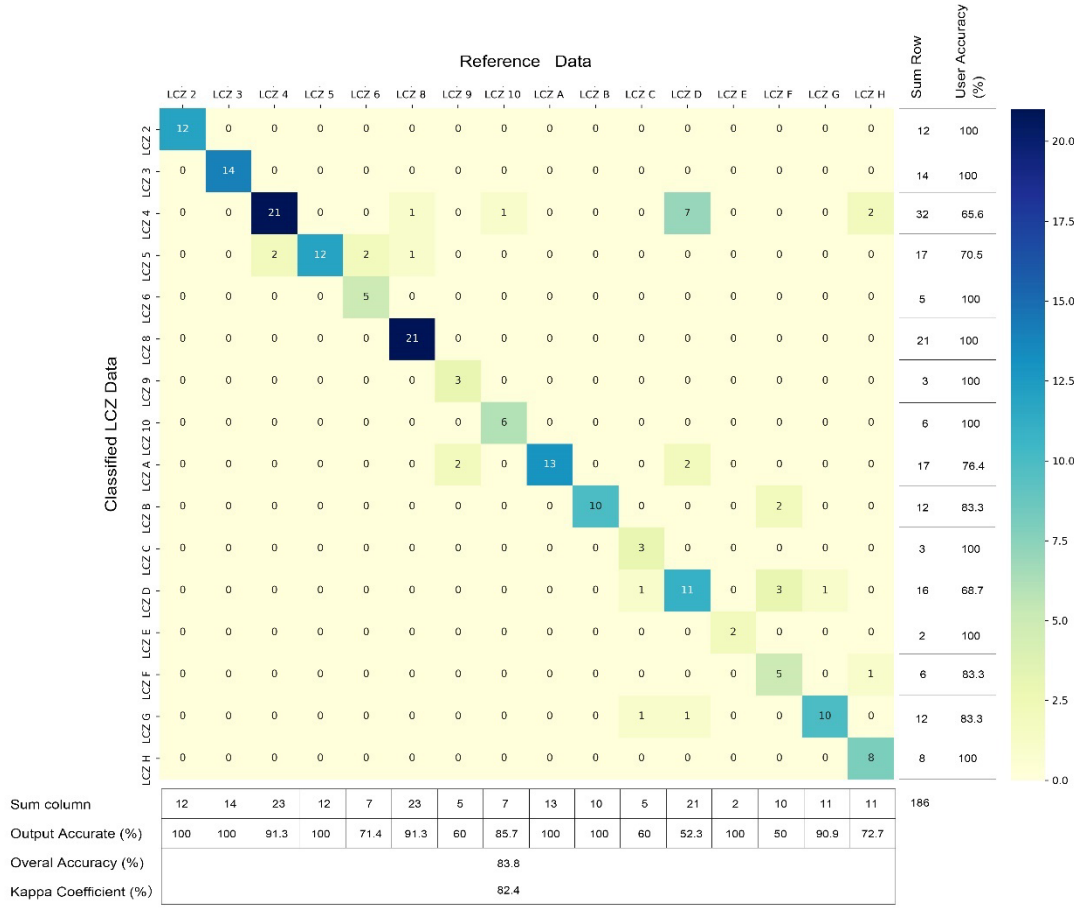

Fig. 6. Confusion matrix for each class of LCZs. The major diagonal (color bar) indicates the agreement between sample data and classified LCZ data

3.2 Day/night seasonal differences of LST in LCZs

3.2.1 Variation of LST in LCZs

LST in LCZs was further investigated to identify the heterogeneity of LST between LCZ types. Table 4 showed the ANOVA results of day/night seasonal LST in LCZs. The p-values of ANOVA test in day/night seasonal LST in LCZs were 0.000 which were lower than the significance level, and suggested that the rejection of null hypotheses. The results showed the LST difference between LCZs in day and night time of all seasons.

Table 4 ANOVA test between LST and LCZs in seasonal dan/night

Time	Source of Variation	Sum_sq	df	Mean_sq	F	p-value
Winter day	Between Groups	602.483	17	37.655	40.187	0.000
	Within Groups	3554.050	3793	0.937		
	Total	4156.533	3809			
Winter night	Between Groups	956.954	17	59.810	65.577	0.000
	Within Groups	3459.414	3793	0.912		

Spring day	Total	4416.369	3809			
	Between Groups	9809.312	17	613.082	131.953	0.000
	Within Groups	17623.046	3793	4.646		
Spring night	Total	27432.357	3809			
	Between Groups	977.390	17	61.087	60.426	0.000
	Within Groups	3834.455	3793	1.011		
Summer day	Total	4811.845	3809			
	Between Groups	9955.925	17	622.245	235.899	0.000
	Within Groups	9999.745	3793	2.638		
Summer night	Total	19955.671	3809			
	Between Groups	1150.528	17	71.908	97.458	0.000
	Within Groups	2798.616	3793	0.738		
Autumn day	Total	39493143	3809			
	Between Groups	2248.117	17	140.507	158.911	0.000
	Within Groups	3353.270	3793	0.884		
Autumn night	Total	5601.87	3809			
	Between Groups	2656.630	17	166.039	114.329	0.000
	Within Groups	5508.575	3793	1.452		
	Total	8165.205	3809			

Further, Tamhane T2 test was used to show which LCZ type have the significant difference of LST. As Fig. 7 shows, the difference of LST between most LCZ types were significant in day/night seasonal time. The overall percentage of comparison within LCZs showing a significant difference in daytime of winter, summer and autumn is 97.5 %, and the spring one is 95.8 %. The apparent difference percentage in nighttime is 96.7 %, 98.4 %, 95 % and 98.4 % for winter, spring, summer and autumn, respectively. Among all LCZs in Wuhan, LCZ 6 and LCZ 9 were the least differentiated type. The LST in LCZ 6 and LCZ 9 showed no significant difference in summer day/night, autumn day/night and winter day time.

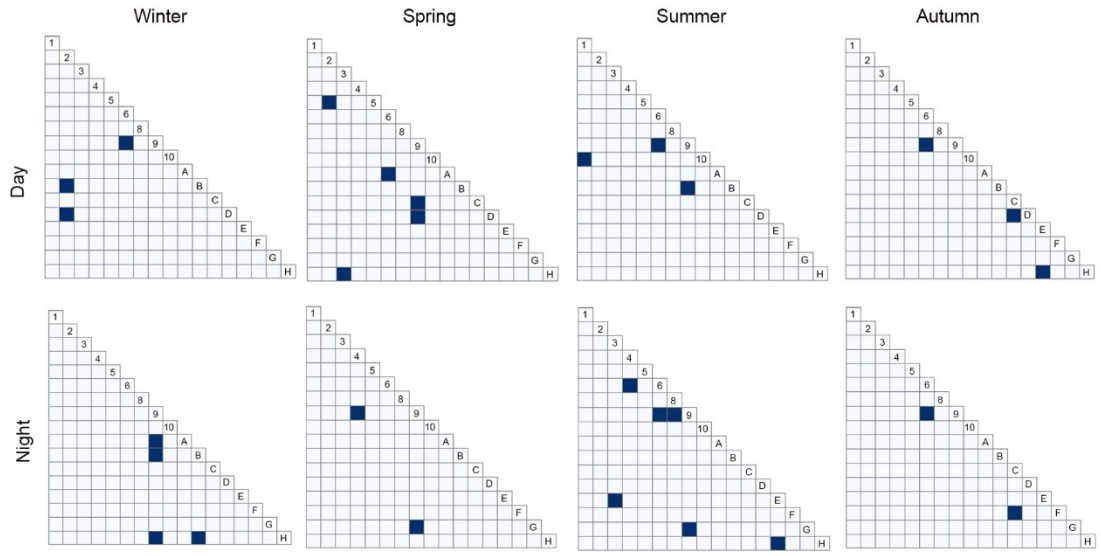

Fig. 7. Tamhane T2 test for all LCZ types (black numbers and letters) in seasonal day/night: white cells represent LCZ pairs where LST was significantly different, mazarine cells represent LCZ pairs which LST was not significantly different.

3.2.2 Day/night seasonal difference of SUHII in LCZs

To illustrate the thermal distribution of LCZs in Wuhan, the day/night seasonal SUHII of LCZs in Wuhan was compared. Differences of the seasonal day SUHII in built classes were obvious in comparison with land cover classes. As Fig. 8 showed, SUHII in spring and summer day in built classes were obviously larger than in winter and autumn day, while the differences became smaller at night. In daytime of all seasons, SUHII within LCZ land cover classes were lower than built classes. In winter, the SUHII differences between land cover classes and built classes was much smaller than other seasons. The reason is that the lower solar radiation in winter caused the lower LST of LCZ built classes, and the weaken heat sinking ability of green space for the dropping vitality of green space (2019). SUHII within LCZs occurred the similar trend in daytime of all seasons. SUHII of LCZ 10 was the strongest one in all seasons with 1.4 °C in winter, 6.5 °C in spring, 6.1 °C in summer and 3.2 °C in autumn due to the large low-rise industry buildings resulting in high human heat activities. The second hottest occurred in LCZ 3 with 0.6 °C in winter, 3.6 °C in spring, 3.9 °C in summer and 1.5 °C in autumn. SUHII within LCZ 8 were stronger than those of LCZ 2, LCZ 4 and LCZ 5 in day of all seasons. Compared with other built classes, the SUHII of LCZ 6 and LCZ 9 were the smallest. SUHII of LCZ G was the smallest among all LCZ type with -0.7 °C in winter, -1.5 °C in spring, -1.1 °C in summer and -0.6 °C in autumn. SUHII of LCZ H in all seasons was similar as those of LCZ 4 and LCZ 5 which showed the thermal character as built classes.

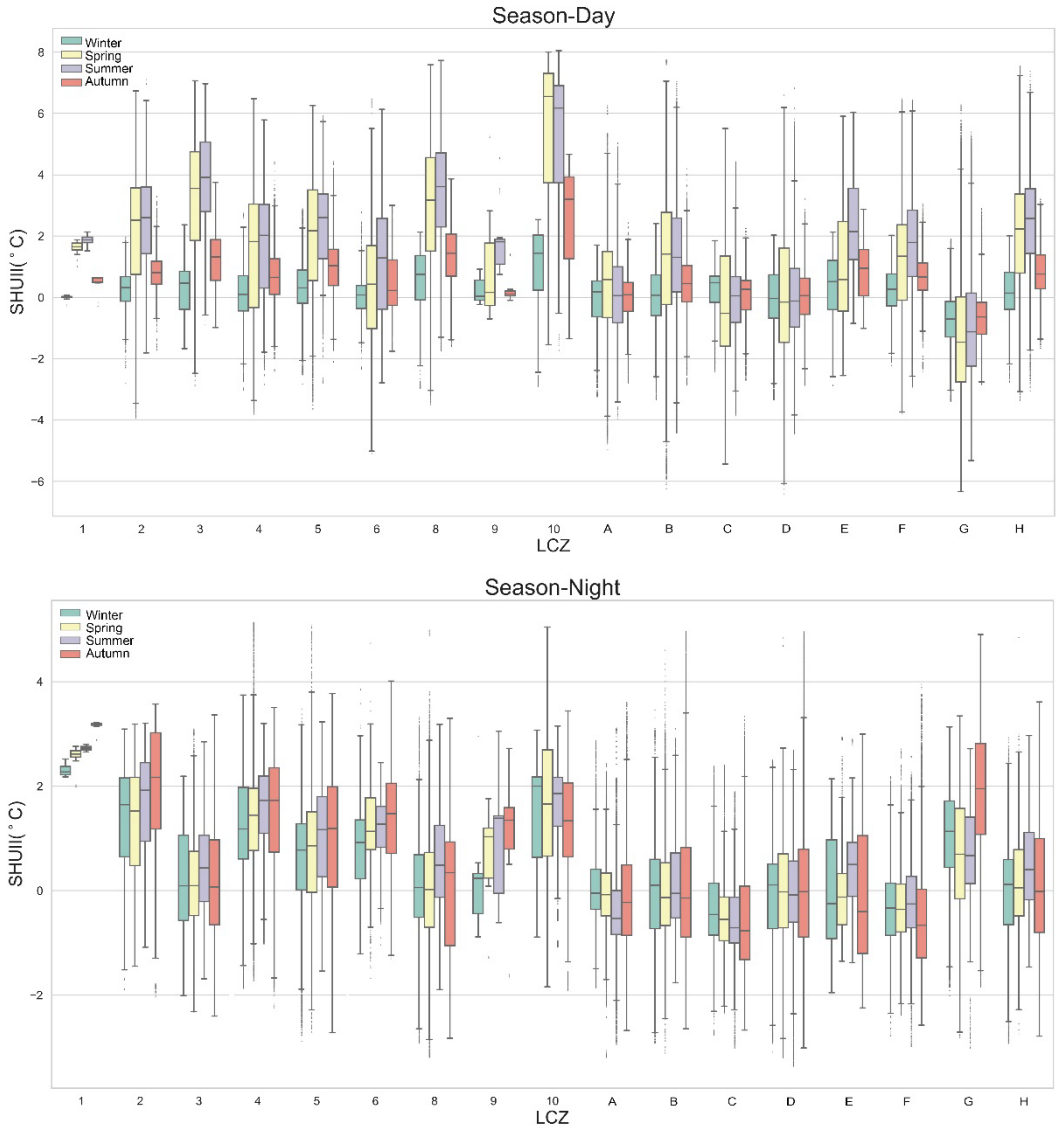

Fig. 8. Box-plots representing SUHII within LCZs for different seasons day/night

The SUHII difference of LCZs in various seasons nighttime was not large (Fig. 8). SUHII in built classes were stronger than most land cover classes. SUHII within LCZs occurred the similar trend at night of all seasons, which were different from daytime. The strongest SUHII occurred in LCZ 1 with 2.2 °C in winter, 2.6 °C in spring, 2.7 °C in summer and 3.2 °C in autumn, and the second strongest SUHII were LCZ 2 and LCZ 10 with 1.6 °C and 1.9 °C in winter, 1.5 °C and 1.7 °C in spring, 1.9 °C and 1.9 °C in summer, 2.2 °C and 1.3 °C in autumn. The main reason is that areas with high-rise density building in LCZ 1 formed street canyons, which was not conducive to heat dissipation. SUHII within LCZ 4, LCZ 5 and LCZ 6 were high and a little lower than LCZ 2. SUHII of LCZ 3 and LCZ 8 were the lowest among built classes at night of all seasons. Contrary to daytime, SUHII of LCZ G was 1.1 °C in winter, 0.7 °C in spring, 0.7 °C in summer and 1.9 °C in autumn, which was much stronger than other land over classes for the water heat dissipation at night.

Comparing all the seasons, the stronger SUHII showed in summer and spring, while the least showed in winter. Regardless the differences of seasons and day/night, the stronger

SUHII were generally displayed in LCZ 2, LCZ 4, LCZ 5 and LCZ 10.

3.2.2 SUHII of LCZs in three districts

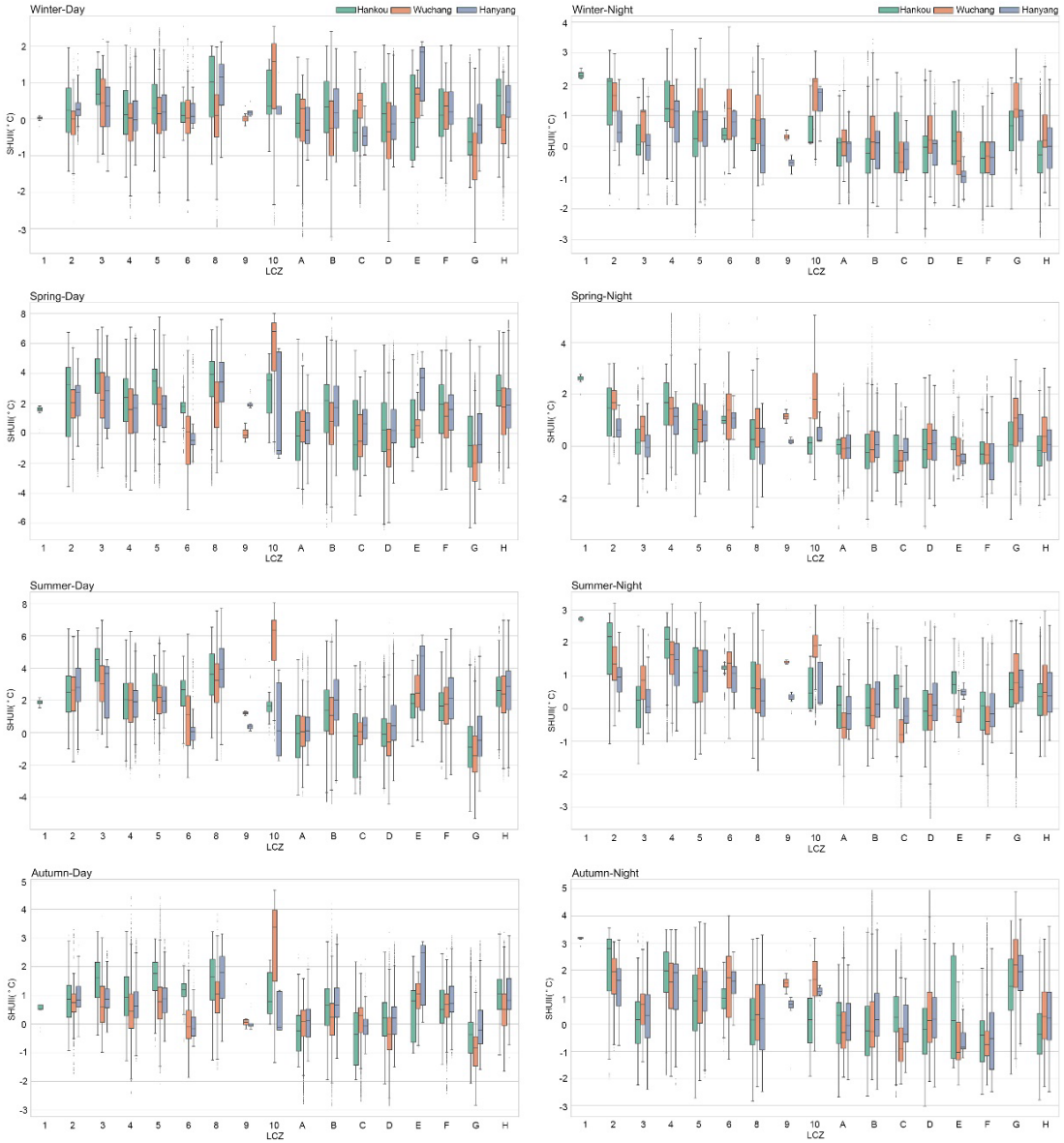

Fig. 9. SUHII within LCZs in three districts for different seasons day/night

To detect the thermal environment within the same LCZ type, the SUHII of LCZs within three districts was compared. As Fig. 9 shows, SUHII within the same LCZ type was different in three districts, and the difference varies depending on the seasons and day/night.

In winter day, the biggest variation of SUHII in three districts showed in LCZ 8, LCZ 10, LCZ E, but occurred various thermal environment in three districts. The highest SUHII within LCZ 8 was in Hanyang 1.2 °C followed by Hanyou 1 °C, and lowest was 0.1 °C in Wuchang. SUHII within LCZ 10 in Wuchang was 1.6 °C, which was much higher than those in Hankou and Hanyang for the biggest industry area in Wuchang. The highest SUHII within LCZ E was in Hanyang 1.9 °C followed by Wuchang 0.7 °C, and lowest was -0.1 °C in Hankou. Small

variation of SUHII in three districts occurred in LCZ 2, LCZ 3, LCZ4, LCZ5, LCZ 6, and SUHII within LCZ 2 - LCZ 6 in Hankou showed slightly higher than Hangyang and Wuchang. However, in winter night, the SUHII difference within LCZ 2, LCZ 3, LCZ 5 and LCZ 6 in three districts became larger than in daytime, while SUHII difference within land cover classes in three districts showed smaller than daytime. The biggest SUHII differences in three districts occurred in LCZ 10 with 2.1 °C in Wuchang, 1.8 °C in Hanyang and 0.2 °C in Hankou. The smallest difference in three districts occurred in LCZ F.

In spring daytime, SUHII difference in three districts became evident among LCZs. As Fig. 9 shows, SUHII difference in three districts within LCZ 2 to LCZ 6 was larger than winter daytime, and SUHII within LCZ 2 to LCZ 8 in Hankou was stronger than those Hanyang and Wuchang. Just as winter daytime, significant differences in three districts occurred in LCZ 10 with 7 °C in Wuchang, 3.9 °C in Hanyou and -1.2 °C in Hanyang. It was noticed that SUHII difference in three districts in spring night was smaller than daytime. The biggest SUHII difference in three districts occurred in LCZ 10 as same as winter night. Slightly SUHII difference in three districts occurred in LCZ A, LCZ B, LCZ C, LCZ D and LCZ F.

In summer daytime, SUHII difference within most LCZs in three districts became smaller than spring daytime. Small difference in three districts occurred in LCZ 2, LCZ 5 and LCZ A. SUHII within LCZ 3, LCZ 4 and LCZ 6 in Hankou was higher than in Wuchang and Hanyang. The biggest SUHII difference in three districts occurred in LCZ 10 with 6.5 °C in Wuchang, 1.8 °C in Hankou and 0.1 °C in Hanyang, which was similar to spring daytime. Similar as in spring night, SUHII difference in three districts in summer night was smaller than daytime. The significant difference occurred in LCZ 10, LCZ A, LCZ C and LCZ E. SUHII within LCZ 10 in Wuchang was higher than Hankou followed by Hanyang as same as winter and spring night. SUHII within LCZ A, LCZ C and LCZ E in Hankou was stronger than Hanyang followed by Wuchang.

In autumn daytime, SUHII difference within most LCZs in three districts was similar to summer daytime and the difference became furtherly smaller. SUHII within LCZ 2- LCZ 6 in Hankou was higher than in Wuchang and Hanyang. The biggest SUHII differences in three districts occurred in LCZ 10 with 3.4 °C in Wuchang, 0.8 °C in Hankou and -0.9 °C in Hanyang, which was smaller than summer and spring daytime but higher than winter daytime. The smallest difference in three districts occurred in LCZ 3 and LCZ F. In autumn nighttime, SUHII difference in three districts among LCZs became smaller than daytime. The biggest SUHII difference in three districts still occurred in LCZ 10 with 1.7 °C in Wuchang, 0.2 °C in Hankou and 1.2 °C in Hanyang, which was much smaller than daytime. SUHII within LCZ 2, LCZ 4, LCZ A, LCZ C and LCZ E in Hankou was stronger than Hanyang followed by Wuchang, which was similar to summer nighttime.

Comparing all the seasons, the significant SUHII difference in three districts within LCZs occurred in summer and spring daytime, while the least showed in winter daytime. Disregarding the differences of seasons and day/night, the highest SUHII difference in three districts was generally displayed in LCZ 10. The significant SUHII difference within the same LCZ type in three districts further confirmed that the spatial pattern of LCZs had an impact on thermal environment in Urban area.

3.3 The relationship between SUHII and LCZs spatial pattern

The Ordinary Least Squares model (OLS) in ArcGIS was used to identify the relation between day/night seasonal SUHII and landscape metrics. Adjust R^2 in day seasonal OLS regression model was 0.31, 0.617, 0.741, 0.614 for winter, spring, summer and autumn, and was 0.483, 0.394, 0.531 and 0.63 at night (Table 5). These indicated that landscape metrics were statistically and significantly related with SUHII in regression models in spring daytime, summer and autumn day/night. VIF of each indicator was listed in Table 6, and were all below 10, with a maximum of 2.544 and a minimum of 1.075. This demonstrated that there was no multicollinearity among the selected landscape metrics.

Table 5 Adjust R^2 of OLS regression models.

	Winter	Spring	Summer	Autumn
Day	0.310**	0.617**	0.741**	0.614**
Night	0.483**	0.394**	0.531**	0.630**

Note: ** represents $p < 0.01$ in the significance test.

Table 6 Results of collinearity between landscape indicators.

Variable	VIF	Variable	VIF	Variable	VIF	Variable	VIF
PLAND_2	1.075	PLAND_4	1.357	PLAND_5	1.343	PLAND_8	1.269
PLAND_D	2.471	PLAND_G	1.692	PLAND_H	1.223	COHISON	1.531
SHAPE_AM	1.646	SHDI	2.544				

Then Global Moran's I in ArcGIS was used to test the spatial autocorrelation hypothesis with the results been listed in Table 7. It can be seen that the Moran I value for SUHII of all OLS model was strongly significant at the 0.001 level and had positive z-score values, which identified the high spatial autocorrelation. Thus, the GWR model was used in the study and all variables were processed for data standardization in SPSS to eliminate the influence of dimension.

Table 7 Spatial autocorrelation results.

Model	Moran I	Z-Score	P-Value
Winter Day	0.768	37.863	0.000
Winter Night	0.557	27.499	0.000
Spring Day	0.630	31.063	0.000
Spring Night	0.664	32.762	0.000
Summer Day	0.581	28.674	0.000
Summer Night	0.722	35.587	0.000
Autumn Day	0.673	32.227	0.000
Autumn Night	0.636	31.387	0.000

Table 8 showed the results of GWR model. The parameter R^2 and adjust R^2 were all above 0.7 and the range of Akaike Information Criterion (AICc) was about from 1286.818 to 2599.119, which indicated that GWR model was fitness to be used in this study. Based on adjust R^2, it can be seen that the influence of LCZ spatial pattern on SUHII from high to low was summer, autumn, spring and winter. The same phenomenon occurred in both seasonal day and night.

From the coefficient aspect, most coefficients of PLAND were larger than those of CONTAG, SHAMP_AM and SHDI in day and night of all seasons, which demonstrated PLAND had a stronger impact on SUHII.

PLAND_8 had a positive relation with SUHII and had high coefficients in daytime of all seasons, which were 0.226 in winter, 0.208 in spring, 0.214 in summer and 0.277 in autumn. This indicated high temperature aggravate with the increasing PLAND_8 in daytime of all seasons. However, coefficients of PLAND_8 became smaller at night indicating the weaker impact of LCZ 8 on increasing SUHII at night. PLAND_4 had a positive relation with SUHII and the coefficient from winter to autumn was 0.08, 0.193, 0.221 and 0.204, respectively. This showed with LCZ 4 area increasing, the high temperature would become more serious in summer and autumn, less serious in spring and little increase in winter. Contrary to LCZ 8, LCZ 4 in winter, spring and summer showed stronger impact on enhancing SUHII at night.

The effects of PLAND_2 and PLAND_5 on urban thermal environment showed significant seasonal differences. PLAND_2 had a positive relation with SUHII in spring, summer and autumn day and the coefficient was 0.064, 0.165, 0.105, respectively, which were smaller than PLAND_8 and PLAND 4. In spring and summer day, PLAND_5 also had a positive relation with SUHII and the coefficient was 0.057, 0.119, respectively, which were smaller than PLAND_2, PLAND_8 and PLAND 4. These explained that PLAND_2 and PLAND_5 had the heating impact on urban environment in spring and summer day, but the influence was smaller than those of PLAND_8 and PLAND_4. Similar to LCZ 4, coefficients of PLAND_2 and PLAND_5 became larger than season daytime. The strongest impact on increasing SUHII at night was LCZ 2 with 0.281 in winter, 0.331 in spring, 0.417 in summer and 0.242 in Autumn. PLAND_H had a positive relation with SUHII in day/night of all seasons, but the coefficient was much smaller than other built classes. This demonstrated that LCZ H had less impact on intensified urban heat islands in comparison with LCZ 2, LCZ 4, LCZ 5 and LCZ 8.

In daytime, PLAND_G and PLAND_D had a negative relation with SUHII. The coefficients of PLAND_G were 0.381, 0.497, 0.472, 0.564 for winter, spring, summer and autumn, respectively. The coefficients of PLAND_D were a little smaller and were 0.128, 0.318, 0.303, 0.344 from winter to autumn. These demonstrated that high temperature would be mitigated by increasing PLAND_G and PLAND_D, and cooling effect of LCZ G was much stronger than LCZ D in daytime. Results also showed that PLAND_G at night still had a negative relation with SUHII in spring, summer and autumn, but had a positive relation with SUHII in winter. This is because sometimes in winter it was very cold with the temperature under zero, and water had a higher temperature than surroundings resulting in increasing SUHII. The coefficient of PLAND_G at night was a bit lower except autumn than daytime, and they were all larger than PLAND_D.

Table 8 Statistical description of GWR mean coefficient.

	Day				Night			
	Winter	Spring	Summer	Autumn	Winter	Spring	Summer	Autumn
PLAND_2	0.002	0.064	0.165	0.105	0.281	0.331	0.417	0.242
PLAND_4	0.080	0.193	0.221	0.204	0.226	0.221	0.299	0.194

PLAND_5	0.154	0.057	0.119	0.071	0.164	0.215	0.249	0.205
PLAND_8	0.226	0.208	0.214	0.277	0.067	0.038	0.078	0.038
PLAND_D	-0.128	-0.318	-0.303	-0.344	-0.012	-0.016	-0.078	-0.051
PLAND_G	-0.381	-0.497	-0.472	-0.564	0.306	-0.297	-0.278	-0.572
PLAND_H	0.022	0.113	0.098	0.078	0.018	0.033	0.062	0.019
CONTAG	0.063	0.033	0.056	0.043	0.004	0.078	0.003	0.028
SHAPE_AM	-0.061	-0.025	-0.031	-0.024	-0.045	-0.097	-0.048	-0.042
SHDI	-0.077	-0.014	-0.059	-0.005	-0.119	-0.143	-0.054	-0.109
INTERCEPT	-0.0124	0.083	0.097	0.055	0.009	0.111	0.18	0.056
R2	0.812	0.842	0.885	0.86	0.764	0.765	0.866	0.857
Adj.R2	0.768	0.805	0.858	0.827	0.708	0.71	0.834	0.823
AICc	1911.756	2599.119	1286.818	1540.976	2203.753	2195.769	1487.675	1571.094

Results showed that CONTAG had positive relation with SUHII, but SHDI and SHAPE_AM had negative relation with SUHII. Among the three indexes, the coefficients of SHDI were a little larger than CONTAG and SHAPE_AM, and the coefficients of SHDI at night were 0.119 in winter, 0.143 in spring, 0.054 in summer and 0.109 in autumn which were higher than daytime. These mean that types of LCZ had stronger impact on SUHII than aggregation and shape of LCZs, and more LCZ types in space unit would decrease SUHII especial at night.

4.Discussion

4.1 SUHII within LCZs in day/night of all seasons in Wuhan 2020

SUHII within LCZs in Wuhan 2020 showed the seasonal difference especially during daytime. In daytime, stronger SUHII within LCZs in Wuhan 2020 occurred in spring and summer, while the least showed in winter. These were consistent with the studies in Nanjing, Shanghai, Hangzhou in China and central European cities (Geletič et al., 2019; Ma et al., 2021). SUHII seasonal difference became smaller at night in comparison with daytime. SUHII in built classes were generally stronger than land cover classes especially at night of all seasons, and SUHII difference among LCZ built classes became larger at night than daytime. These were similar to results from previous studies (Han, Luo, Liu, Zhang, & Yang, 2022; Unal Cilek & Cilek, 2021). In densely build areas (LCZ 1- LCZ 3), SUHII in daytime of all seasons was stronger with the height decrease but became smaller at night of all the seasons. The main reason was that high-rise buildings caused more shaded space in daytime resulting in lower temperature, while blocked heat diffusion at nighttime. Similar results can be seen in open built area (LCZ 4- LCZ 5). However, it was noticed that SUHII of LCZ 6 was lower than LCZ 5 in daytime and

was slightly higher than LCZ 5 at nighttime. This was because most LCZ 6 in Wuhan is located near the water (lakes or rivers). Water with lower temperature cooled the LCZ 6 in daytime, while water with higher temperature warmed the LCZ 6 at night.

Similar to SUHII among LCZs, significant SUHII difference within LCZs in three districts occurred in spring and summer, while it was least in winter. In three districts, SUHII within the same LCZs showed some difference in various season day/night time. In daytime, SUHII within LCZ 2 - LCZ 6 in Hankou was higher than Wuchang and Hanyang due to the largest PLAND of LCZ 2, LCZ 4, higher CONTAG, and lowest SHDI in Hankou (Fig. 10), while SUHII within LCZ 3, LCZ 5, LCZ 6 in Wuchang was higher than Hankou and Hanyang in nighttime due to the largest PLAND of LCZ 5, LCZ 6 (Fig. 10), and most LCZ 3 clustered around LCZ 5 in Wuchang (Fig. 5). SUHII within LCZ 10 in Wuchang was always higher than Hankou and Hanyang because of the largest PLAND of LCZ 10 in Wuchang. SUHII within LCZ G in Wuchang was the lowest in daytime but the highest at nighttime. All results showed that various composition and configuration of LCZs in Wuchang, Hanyang and Hankou had influences on SUHII of the same LCZ.

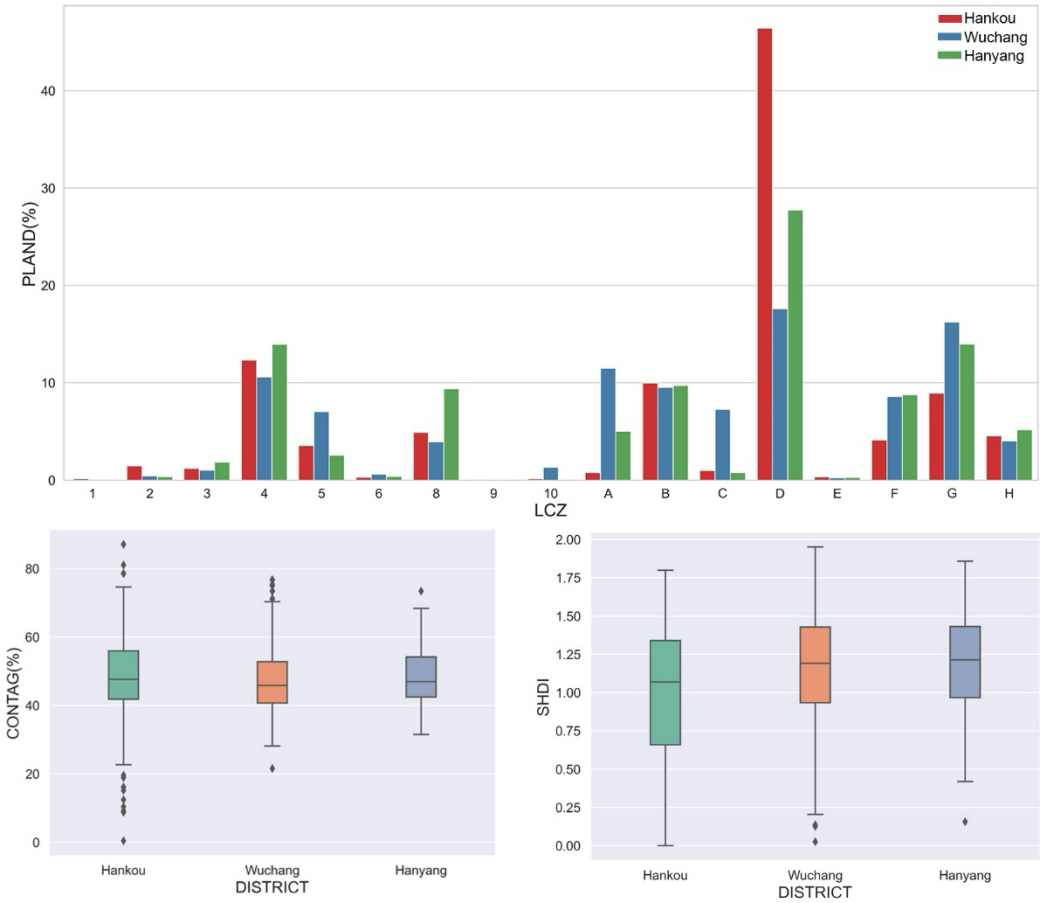

Fig. 10. PLAND, CONTAG, and SHDI of LCZs in three districts.

4.2 The impacts of LCZs spatial pattern on thermal environment

For LCZ types with significant impact on thermal environment, landscape metrics of PLAND, CONTAG, SHDI and SHAPE_AM were applied to detect its impact on SUHII. PLAND of LCZs represented the composition of LCZs and other three metrics represented the

configuration of LCZs within the analysis unit. In Wuhan, LCZ 2, LCZ4, LCZ 5, LCZ 8 and LCZ H had strong positive correlation with SUHII, which were the main heat sources. This was consistent with previous work (Chang et al., 2021; Simanjuntak et al., 2019). LCZ D and LCZ G had strong negative correlation with SUHII, which were the cool sources. This was different to other study which defined the LCZ A and LCZ G as the cool island (Li et al., 2022). The reason was that the previous study defined the cool effects based on the lower LST of LCZ A. In Wuhan, LST of LCZ A was lower than LCZ D. However, the area of LCZ D was much larger than LCZ A in Wuhan resulting in more influence on thermal environment.

PLAND of LCZs had more impact on SUHII than CONTAG, SHDI and SHAPE_AM, which illustrated that the area of heat sources or cool sources had apparent effects on SUHII. Similar results can be found in Nanjing, China (Zihao & Ziyu, 2022). Results also showed that the impacts of spatial pattern of LCZs on SUHII would be affected by diurnal and seasonality. In daytime, LCZ 8 were the main factor for the thermal stress in all the seasons, while at night LCZ 2, LCZ4, LCZ 5 were the main LCZs causing the strong SUHII. The reason was that the large low-rise buildings in LCZ 8 formed large roof surface and open paved surface causing increasing solar radiation absorption in daytime and fast heat diffusion at night. On the contrary, high-rise or mid-rise buildings formed the shady in daytime and blocked the heat diffusion at night (Li et al., 2022). LCZ D and LCZ G had a cooling effect on the environment. LCZ D in winter had a weaker cooling effect on the environment than other three seasons for the lower vitality of green land. In daytime, LCZ G had a stronger cooling impact on SUHII than LCZ D in all the seasons. Both LCZ G and LCZ D at night had a weaker cooling effect than in daytime of all seasons and LCZ G still had a stronger cooling impact than LCZ D in spring, summer and autumn. But LCZ G at winter night showed the positive impact on SUHII, which mean water increased SUHII at winter night. Similar results can be found in the study of Bandung, Indonesia (Simanjuntak et al., 2019).

Results showed that SHDI of LCZs had a slightly stronger impact on SUHII than CONTAG and SHAPE_AM in day/night of all seasons, and SHDI had negative correlation with SUHII. These demonstrated that in analysis unit, the LCZ type richness had more impact on thermal environment than the shape and aggregation of the LCZ, and the single LCZ type especially LCZ built classes would enhance high temperature. This was consistent with results in Nanjing, China (Zihao & Ziyu, 2022). Though the mean coefficient of CONTAG and SHAPE_AM showed the positive and negative correlation with SUHII, more information of CONTAG and SHAPE_AM influencing on SUHII can be seen in Fig. 11. As results of summer day showed, when the LCZ with high temperature was concentrated in analysis unit, higher CONTAG would cause more serious SUHII which occurred in north of Wuchang for the huge area of industry, east and west boundary for the large construction land. When the LCZ with lower temperature was concentrated in the analysis unit, higher CONTAG would mitigate SUHII which occurred in the lake area of Wuchang and Hanyang. These were consistent with previous studies (Simanjuntak et al., 2019; Y. Wang et al., 2017). Similar results occurred in SHAPE_AM. Very regular shape built-up areas increased the SUHII, while less fragmented green-blue areas decreased the SUHII.

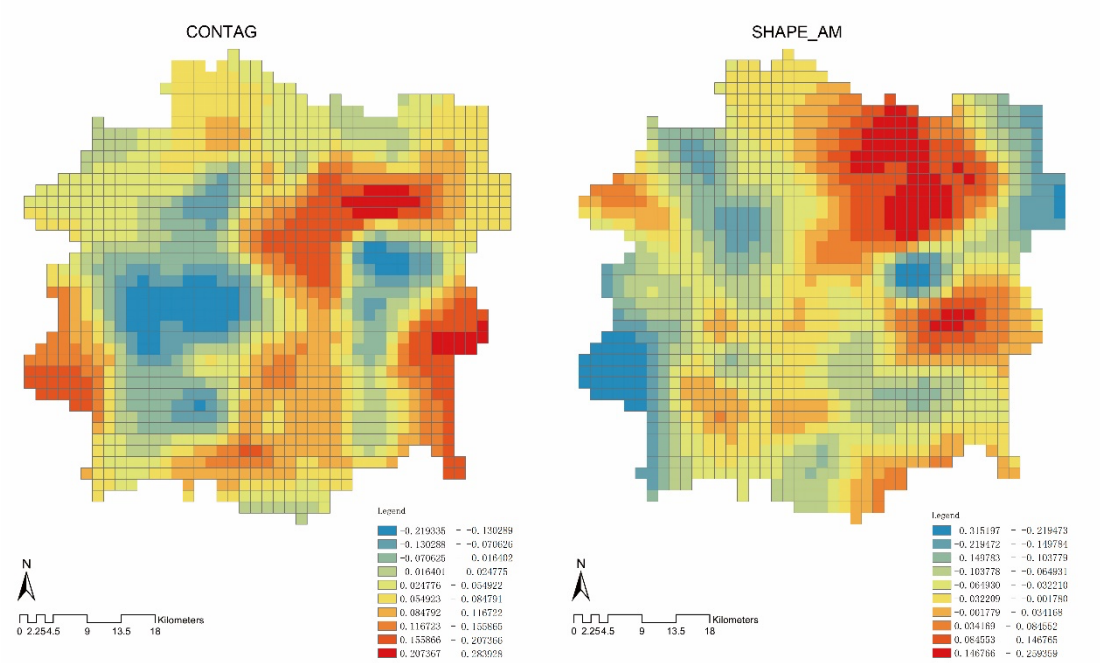

Fig. 11. GWR mean coefficients of CONTAG and SHAPE_AM in summer daytime.

4.3 Strategies to improve Wuhan thermal environment in future development

Results showed that LCZ was suitable to describe the thermal environment in Wuhan. LCZ 2, LCZ 4, LCZ 5, LCZ 8 and LCZ H had strong correlation with SUHII and the PLAND of LCZ 2, LCZ 4, LCZ 5, LCZ 8 had significant impact on increasing SUHII. These results suggest that future development should be controlled in the area of LCZ 2, LCZ 4, LCZ 5 and LCZ 8. For built-up areas, effective cooling measures such as planting trees, replacing pavement or roof material can firstly be applied to the LCZ 2, LCZ 4, LCZ 5 and LCZ 8 to mitigate the thermal environment. It can be noticed that LCZ H covering 4.3% would become built-up area in the future, which has the possibility of exacerbating SUHII. The government should pay attention to the severe urban heat islands in the future, and should prepare compensation and adjustment measures in advance to provide more comfortable thermal environment.

LCZ D and LCZ G had a significant cooling effect on thermal environment, which demonstrated the area of LCZD and LCZ G should be protected and avoid shrinking. Though LCZ A and LCZ B had lower temperature than LCZ built classes, limited cooling effects occurred in Wuhan for the small area of LCZ A and LCZ B. Green space and trees also should be enlarged in built-up areas to mitigate SUHII especially in warm seasons.

SUHII difference of same LCZ type in three districts confirmed that the configuration of LCZs had an impact on SUHII. Mixed LCZ type especially mixed layout of LCZ built classes and land cover classes would help decrease SUHII. Less concentrated and more irregular shape of LCZ built classes, or more connected and less fragment land cover classes would mitigate SUHII. According to these results, urban design and urban development intensity could be optimized for the better thermal environment in Wuhan.

5. Conclusion

This study mapped LCZs in Wuhan in 2020 based on WUDAPT, and detected the SUHII

within LCZs in day/night of all the seasons through MODIS LST data. The landscape metrics PLAND, CONTAG, SHDI and SHAPE_AM were used to explore the impacts of composition and configuration within LCZs on SUHII by GWR model. The results highlighted the following.

LCZs map can be used to describe the thermal environment across all seasons in Wuhan. SUHII difference among LCZs in Wuhan was stronger in spring and summer, and less in winter. SUHII within built classes were stronger than land cover classes. SUHII difference of the same LCZ was found in three districts. SUHII of most other built classes in Hankou were higher than Wuchang and Hanyang. LCZ 2, LCZ 4, LCZ 5, LCZ 8 and LCZ H had a significant aggravating effect on SUHII and LCZ D and LCZ G had an apparently cooling effect on SUHII.

Composition and configuration of LCZs in Wuhan had influences on SUHII of the same LCZ. PLAND of LCZs had more impacts on SUHII than CONTAG, SHDI and SHAPE_AM. SHDI richness of LCZs in analysis unit helped alleviate SUHII. High CONTAG of LCZ with high LST increased SUHII, while High CONTAG of LCZ with low LST decreased SUHII. Very regular shape of LCZ built classes increased the SUHII, while less fragmented of LCZ land cover classes decreased the SUHII.

In future study, the spatial pattern of LCZs with low SUHII can be detected. The following research could furtherly explore the optimal composition and configuration of LCZs for a better urban thermal environment, and identify the optimum values of main landscape metrics of LCZs. These would help to guild the future development or update in Wuhan to build a comfortable living environment.

Acknowledgments

This research is supported by State Scholarship Fund in China (No. 202006765009) and the Fundamental Research Funds for the Central Universities (No. 2662018JC045).

References

Andrew Freedman. (2022, August 22). China's unrivaled 70-day heat wave. Axios. Retrieved from https://www.axios.com/

Anjos, M., Targino, A. C., Krecl, P., Oukawa, G. Y., & Braga, R. F. (2020). Analysis of the urban heat island under different synoptic patterns using local climate zones. *Building and Environment, 185*. doi:10.1016/j.buildenv.2020.107268

Aslam, A., & Rana, I. A. (2022). The use of local climate zones in the urban environment: A systematic review of data sources, methods, and themes. *Urban Climate, 42*. doi:10.1016/j.uclim.2022.101120

Bechtel, B., Alexander, P. J., Beck, C., Böhner, J., Brousse, O., Ching, J., . . . Xu, Y. (2019). Generating WUDAPT Level 0 data – Current status of production and evaluation. *Urban Climate, 27*, 24-45. doi:10.1016/j.uclim.2018.10.001

Beck, C., Straub, A., Breitner, S., Cyrys, J., Philipp, A., Rathmann, J., . . . Jacobeit, J. (2018). Air temperature characteristics of local climate zones in the Augsburg urban area (Bavaria, southern Germany) under varying synoptic conditions. *Urban Climate, 25*, 152-166. doi:10.1016/j.uclim.2018.04.007

Chang, Y., Xiao, J., Li, X., Middel, A., Zhang, Y., Gu, Z., . . . He, S. (2021). Exploring diurnal thermal variations in urban local climate zones with ECOSTRESS land surface temperature data. *Remote Sensing of Environment, 263*. doi:10.1016/j.rse.2021.112544

Chen, X., Yang, J., Ren, C., Jeong, S., & Shi, Y. (2021). Standardizing thermal contrast among local climate zones at a continental scale: Implications for cool neighborhoods. *Building and Environment, 197*. doi:10.1016/j.buildenv.2021.107878

Dewan, A., Kiselev, G., Botje, D., Mahmud, G. I., Bhuian, M. H., & Hassan, Q. K. (2021). Surface urban heat island intensity in five major cities of Bangladesh: Patterns, drivers and trends. *Sustainable Cities and Society, 71*. doi:10.1016/j.scs.2021.102926

Du, P., Chen, J., Bai, X., & Han, W. (2020). Understanding the seasonal variations of land surface temperature in Nanjing urban area based on local climate zone. *Urban Climate, 33*. doi:10.1016/j.uclim.2020.100657

Eldesoky, A. H. M., Gil, J., & Pont, M. B. (2021). The suitability of the urban local climate zone classification scheme for surface temperature studies in distinct macroclimate regions. *Urban Climate, 37*. doi:10.1016/j.uclim.2021.100823

Emery, J., Pohl, B., Crétat, J., Richard, Y., Pergaud, J., Rega, M., . . . Thévenin, T. (2021). How local climate zones influence urban air temperature: Measurements by bicycle in Dijon, France. *Urban Climate, 40*. doi:10.1016/j.uclim.2021.101017

Gao, Y., Zhao, J., & Han, L. (2022). Exploring the spatial heterogeneity of urban heat island effect and its relationship to block morphology with the geographically weighted regression model. *Sustainable Cities and Society, 76*. doi:10.1016/j.scs.2021.103431

Geletič, J., Lehnert, M., Savić, S., & Milošević, D. (2019). Inter-/intra-zonal seasonal variability of the surface urban heat island based on local climate zones in three central European cities. *Building and Environment, 156*, 21-32. doi:10.1016/j.buildenv.2019.04.011

Gu, Y., & You, X.-y. (2022). A spatial quantile regression model for driving mechanism of urban heat island by considering the spatial dependence and heterogeneity: An example of Beijing, China. *Sustainable Cities and Society, 79*. doi:10.1016/j.scs.2022.103692

Han, B., Luo, Z., Liu, Y., Zhang, T., & Yang, L. (2022). Using Local Climate Zones to investigate Spatio-temporal evolution of thermal environment at the urban regional level: A case study in Xi'an, China. *Sustainable Cities and Society, 76*. doi:10.1016/j.scs.2021.103495

Hay Chung, L. C., Xie, J., & Ren, C. (2021). Improved machine-learning mapping of local climate zones in metropolitan areas using composite Earth observation data in Google Earth Engine. *Building and Environment, 199*. doi:10.1016/j.buildenv.2021.107879

Hidalgo, J., Dumas, G., Masson, V., Petit, G., Bechtel, B., Bocher, E., . . . Mills, G. (2019). Comparison between local climate zones maps derived from administrative datasets and satellite observations. *Urban Climate, 27*, 64-89. doi:10.1016/j.uclim.2018.10.004

Huang, Q., Huang, J., Yang, X., Fang, C., & Liang, Y. (2019). Quantifying the seasonal contribution of coupling urban land use types on Urban Heat Island using Land Contribution Index: A case study in Wuhan, China. *Sustainable Cities and Society, 44*, 666-675. doi:10.1016/j.scs.2018.10.016

Jin, L., Pan, X., Liu, L., Liu, L., Liu, J., & Gao, Y. (2020). Block-based local climate zone approach to urban climate maps using the UDC model. *Building and Environment, 186*. doi:10.1016/j.buildenv.2020.107334

Kim, M., Jeong, D., & Kim, Y. (2021). Local climate zone classification using a multi-scale, multi-level attention network. *ISPRS Journal of Photogrammetry and Remote Sensing, 181*, 345-366. doi:10.1016/j.isprsjprs.2021.09.015

Kotharkar, R., Ghosh, A., & Kotharkar, V. (2021). Estimating summertime thermal phenomenon in

a tropical Indian city using Local Climate Zone (LCZ) framework. *Urban Climate, 36*. doi:10.1016/j.uclim.2021.100784

Li, X., Stringer, L. C., & Dallimer, M. (2022). The role of blue green infrastructure in the urban thermal environment across seasons and local climate zones in East Africa. *Sustainable Cities and Society, 80*. doi:10.1016/j.scs.2022.103798

Liu, S., & Shi, Q. (2020). Local climate zone mapping as remote sensing scene classification using deep learning: A case study of metropolitan China. *ISPRS Journal of Photogrammetry and Remote Sensing, 164*, 229-242. doi:10.1016/j.isprsjprs.2020.04.008

Lu, B., Charlton, M., Harris, P., & Fotheringham, A. S. (2014). Geographically weighted regression with a non-Euclidean distance metric: a case study using hedonic house price data. *International Journal of Geographical Information Science, 28*(4), 660-681. doi:10.1080/13658816.2013.865739

Ma, L., Yang, Z., Zhou, L., Lu, H., & Yin, G. (2021). Local climate zones mapping using object-based image analysis and validation of its effectiveness through urban surface temperature analysis in China. *Building and Environment, 206*. doi:10.1016/j.buildenv.2021.108348

Nectar Gan. (2022, August 26). China's worst heat wave on record is crippling power supplies. How it reacts will impact us all. CNN. Retrieved from https://edition.cnn.com/

Quan, S. J., & Bansal, P. (2021). A systematic review of GIS-based local climate zone mapping studies. *Building and Environment, 196*. doi:10.1016/j.buildenv.2021.107791

Shi, L., Ling, F., Foody, G. M., Yang, Z., Liu, X., & Du, Y. (2021). Seasonal SUHI Analysis Using Local Climate Zone Classification: A Case Study of Wuhan, China. *Int J Environ Res Public Health, 18*(14). doi:10.3390/ijerph18147242

Simanjuntak, R. M., Kuffer, M., & Reckien, D. (2019). Object-based image analysis to map local climate zones: The case of Bandung, Indonesia. *Applied Geography, 106*, 108-121. doi:10.1016/j.apgeog.2019.04.001

Stewart, I. D., & Oke, T. R. (2012). Local climate zones for urban temperature studies *AMERICAN METEOROLOGICAL SOCIETY, 11*, 1879-1900. doi:10.1175/BAMS-D-i

Ting Chen. (2022, August 11). The provincial meteorological observatory has issued an orange alert. Sichuan Daily. Retrieved from http://sc.wenming.cn/ (In Chinese)

Unal Cilek, M., & Cilek, A. (2021). Analyses of land surface temperature (LST) variability among local climate zones (LCZs) comparing Landsat-8 and ENVI-met model data. *Sustainable Cities and Society, 69*. doi:10.1016/j.scs.2021.102877

Wang, C., Middel, A., Myint, S. W., Kaplan, S., Brazel, A. J., & Lukasczyk, J. (2018). Assessing local climate zones in arid cities: The case of Phoenix, Arizona and Las Vegas, Nevada. *ISPRS Journal of Photogrammetry and Remote Sensing, 141*, 59-71. doi:10.1016/j.isprsjprs.2018.04.009

Wang, J., Qingming, Z., Guo, H., & Jin, Z. (2016). Characterizing the spatial dynamics of land surface temperature–impervious surface fraction relationship. *International Journal of Applied Earth Observation and Geoinformation, 45*, 55-65. doi:10.1016/j.jag.2015.11.006

Wang, R., Wang, M., Zhang, Z., Hu, T., Xing, J., He, Z., & Liu, X. (2022). Geographical Detection of Urban Thermal Environment Based on the Local Climate Zones: A Case Study in Wuhan, China. *Remote Sensing, 14*(5). doi:10.3390/rs14051067

Wang, Y., Zhan, Q., & Ouyang, W. (2017). Impact of Urban Climate Landscape Patterns on Land Surface Temperature in Wuhan, China. *Sustainability, 9*(10). doi:10.3390/su9101700

Wu, J., Liu, C., & Wang, H. (2022). Analysis of Spatio-temporal patterns and related factors of thermal comfort in subtropical coastal cities based on local climate zones. *Building and Environment, 207*. doi:10.1016/j.buildenv.2021.108568

Wu, Y., Hou, H., Wang, R., Murayama, Y., Wang, L., & Hu, T. (2022). Effects of landscape patterns on the morphological evolution of surface urban heat island in Hangzhou during 2000 – 2020. *Sustainable Cities and Society, 79*. doi:10.1016/j.scs.2022.103717

Xu, C., Hystad, P., Chen, R., Van Den Hoek, J., Hutchinson, R. A., Hankey, S., & Kennedy, R. (2021). Application of training data affects success in broad-scale local climate zone mapping. *International Journal of Applied Earth Observation and Geoinformation, 103*. doi:10.1016/j.jag.2021.102482

Yang, J., Jin, S., Xiao, X., Jin, C., Xia, J., Li, X., & Wang, S. (2019). Local climate zone ventilation and urban land surface temperatures: Towards a performance-based and wind-sensitive planning proposal in megacities. *Sustainable Cities and Society, 47*. doi:10.1016/j.scs.2019.101487

Yang, J., Ren, J., Sun, D., Xiao, X., Xia, J., Jin, C., & Li, X. (2021). Understanding land surface temperature impact factors based on local climate zones. *Sustainable Cities and Society, 69*. doi:10.1016/j.scs.2021.102818

Yang, X., Peng, L. L. H., Chen, Y., Yao, L., & Wang, Q. (2020). Air humidity characteristics of local climate zones: A three-year observational study in Nanjing. *Building and Environment, 171*. doi:10.1016/j.buildenv.2020.106661

Yang, X., Yao, L., Jin, T., Peng, L. L. H., Jiang, Z., Hu, Z., & Ye, Y. (2018). Assessing the thermal behavior of different local climate zones in the Nanjing metropolis, China. *Building and Environment, 137*, 171-184. doi:10.1016/j.buildenv.2018.04.009

Yoo, C., Han, D., Im, J., & Bechtel, B. (2019). Comparison between convolutional neural networks and random forest for local climate zone classification in mega urban areas using Landsat images. *ISPRS Journal of Photogrammetry and Remote Sensing, 157*, 155-170. doi:10.1016/j.isprsjprs.2019.09.009

Yusha Zhao, Caiyu Liu, Fandi Cui. (2022, August 14). China witnessing strongest heat wave in six decades; long-lasting high temperatures to become new normal in the future: meteorologists. Global Times. Retrieved from https://www.globaltimes.cn/

Zhang, L., Zhan, Q., & Lan, Y. (2018). Effects of the tree distribution and species on outdoor environment conditions in a hot summer and cold winter zone: A case study in Wuhan residential quarters. *Building and Environment, 130*, 27-39. doi:10.1016/j.buildenv.2017.12.014

Zhao, C., Jensen, J., Weng, Q., Currit, N., & Weaver, R. (2019). Application of airborne remote sensing data on mapping local climate zones: Cases of three metropolitan areas of Texas, U.S. *Computers, Environment and Urban Systems, 74*, 175-193. doi:10.1016/j.compenvurbsys.2018.11.002

Zhou, L., Yuan, B., Hu, F., Wei, C., Dang, X., & Sun, D. (2022). Understanding the effects of 2D/3D urban morphology on land surface temperature based on local climate zones. *Building and Environment, 208*. doi:10.1016/j.buildenv.2021.108578

Zhou, X., Okaze, T., Ren, C., Cai, M., Ishida, Y., & Mochida, A. (2020). Mapping local climate zones for a Japanese large city by an extended workflow of WUDAPT Level 0 method. *Urban Climate, 33*. doi:10.1016/j.uclim.2020.100660

Zhou, X., Okaze, T., Ren, C., Cai, M., Ishida, Y., Watanabe, H., & Mochida, A. (2020). Evaluation of urban heat islands using local climate zones and the influence of sea-land breeze. *Sustainable Cities and Society, 55*. doi:10.1016/j.scs.2020.102060

Zhou, Y., Zhang, G., Jiang, L., Chen, X., Xie, T., Wei, Y., . . . Lun, F. (2021). Mapping local climate zones and their associated heat risk issues in Beijing: Based on open data. *Sustainable Cities and Society, 74*. doi:10.1016/j.scs.2021.103174

Zihao, W., & Ziyu, T. (2022). Study on the correlation between the spatial patterns of urban form and urban thermal environment: a case study of Nanjing. *Journal of Nanjing Normal University(Natural Science Edition), 45*(02), 16-25.